



# Facile Fabrication of Nano-sized SiO<sub>2</sub> by an Improved Sol–Gel Route: As an Adsorbent for Enhanced Removal of Cd(II) and Pb(II) Ions

Hesham H. El-Feky<sup>1</sup> · Mohamed S. Behiry<sup>2</sup> · Alaa S. Amin<sup>1</sup> · Mostafa Y. Nassar<sup>1</sup>

Received: 1 October 2021 / Accepted: 19 December 2021 / Published online: 29 January 2022  
© The Author(s), under exclusive licence to Springer Science+Business Media, LLC, part of Springer Nature 2021

## Abstract

We herein report a direct and facile sol–gel method for the preparation of porous silicon dioxide nanoparticles using dissolved silica gel and nitric acid. We prepared SiO<sub>2</sub> nanoparticles at three different pH values: 6, 7, and 8. The washed and dried products were calcined at 800 °C for 2 h. The average crystallite size of the prepared SiO<sub>2</sub> nanoparticles was ca. 37.7 nm. The products were characterized by using FT-IR, TEM, FE-SEM, and XRD analyses. The as-prepared SiO<sub>2</sub> nanoparticles showed high adsorption capacities; ca. 32.2 mg g<sup>-1</sup> and 42.2 mg g<sup>-1</sup>, for the removal of Pb(II) and Cd(II) ions, respectively, from aqueous media. The adsorption data followed well the pseudo-second-order and Langmuir isotherm models. The determined thermodynamic parameters:  $\Delta G^\circ$  (from -5.026 to -5.180 kJ/mol for Cd(II) ion adsorption and from -5.528 to -5.732 kJ/mol for Pb(II) ion adsorption) and  $\Delta H^\circ$  (-7.00 and -7.607 kJ/mol, respectively), indicate the spontaneous, exothermic, and physisorption nature of the adsorption process. Besides, the excellent reusability and adsorption capacity for SiO<sub>2</sub> nanoparticles revealed their good efficiency for the removal of Pb(II) and Cd(II) ions from aqueous media.

**Keywords** Sol–gel synthesis · SiO<sub>2</sub> nanoparticles · Lead and cadmium · Adsorption · Kinetics · Thermodynamic

## 1 Introduction

One vital challenge worldwide is water contamination by heavy metals, which is considered one of the most toxic water pollutants. Heavy-metal ions are a severe environmental problem due to that toxic waste in water not only poses a major health risk to humankind, but also destroys the circulation of the ecological environment [1]. Due to the non-biodegradable nature, heavy metals get accumulated in the ecosystem and finally enter in food cycle [2, 3]. Among the heavy metal ions, Cd(II) and Pb(II) have been shown to have carcinogenic effects. Heavy metals such as cadmium and lead among others, are commonly detected in industrial effluents [4]. A variety of syndromes, renal function hypertension, hepatic injury, lung damage and teratogenic effects

may result from cadmium toxicity [5]. Lead may cause mental disturbance, retardation, and semi-permanent brain damage [1]. Hence, due to the Cd(II) and Pb(II) potential threat to human health, it is important to control the concentration of these toxic ions from polluted water to provide a safe and clean water supply to the public [4].

So far, several methods have been proposed for the remediation of organic and inorganic pollutants [6, 7] include adsorption [8, 9], chemical precipitation [10, 11], ion exchange [12, 13], membrane filtration [14–18], coagulation [19, 20], photocatalytic degradation [21, 22], and biosorption processes [23–26]. It is notable that most of these methods have one or more drawbacks; however, adsorption method still has the superiority over all methods due to its simplicity, high efficiency, cheapness, and regeneration of the adsorbents [27–29]. Therefore, SiO<sub>2</sub> nanoadsorbent has been suggested for treatment of aqueous solutions from various pollutants [30]. The SiO<sub>2</sub> adsorbent was characterized by low-cost, high-performance, high adsorption capacity, fast adsorption, and good recyclability. Silicon dioxide is considered one of the unique materials with wide applications in water purification [31–33]. Silicon dioxide is an inorganic solid material that is composed of three-dimensional network structures (the silicon atom is covalently

✉ Alaa S. Amin  
asamin2005@hotmail.com

✉ Mostafa Y. Nassar  
m\_y\_nassar@yahoo.com; m\_y\_nassar@fsc.bu.edu.eg

<sup>1</sup> Chemistry Department, Faculty of Science, Benha University, Benha 13518, Egypt

<sup>2</sup> Central Laboratory, Dakahlia Water and Wastewater Company (DWWC), Cairo, Egypt

bonded to four oxygen atoms) joined by a common atom (bridge), which gives structures of porous materials having a large surface area with chemical formula, ( $\text{SiO}_2$ ) [34, 35]. Silicon dioxide materials possess excellent physicochemical properties such as water stability, thermal stability, good mechanical strength and it is nontoxic [30]. Mesoporous silicon dioxide received greater attention during the last couple of decades due to its diverse application in various research areas such as column chromatography, adsorption, drug delivery and immobilization of enzymes or proteins, etc. [36, 37]. Recently, various types of nano-porous silicon dioxide-based materials were found to be efficient in the removal of toxic metals from aqueous solutions depending on its properties such as specific surface area, narrow pore-size distributions and controlled pore sizes [38]. Numerous researchers, in recent times, showed interest in the development of new methodologies for the synthesis of micro and mesoporous silicon dioxide with a special focus on the improvement in surface area, pore size, pore volume, etc. [30, 39]. The physicochemical properties of silicon dioxide are greatly dependent on the synthesis methods, their conditions such as pH of the medium, temperature, source of silicon dioxide, templating agent and its concentrations [40].

Herein, pure nano-sized  $\text{SiO}_2$  was successfully synthesized via a sol–gel route. The structure, textural and morphological characteristics of the synthesized silicon dioxide were investigated. The obtained silicon dioxide was then applied for the adsorption of Cd(II) and Pb(II) ions from polluted aqueous media. The effects of operational parameters on the adsorption efficiency, kinetic, isotherm and thermodynamic aspects of Cd(II) and Pb(II) ions adsorption were explored.

## 2 Materials and Methods

### 2.1 Materials

All reagents were of analytical grade and they were purchased and used as received without further purification. Silica gel of 60/120 (mesh), nitric acid ( $\text{HNO}_3$ , 90%), hydrochloric acid ( $\text{HCl}$ , 37%), sodium hydroxide ( $\text{NaOH}$ , 98%), cadmium chloride ( $\text{CdCl}_2 \cdot 4\text{H}_2\text{O}$ , 99.9%) and lead nitrate ( $\text{Pb}(\text{NO}_3)_2$ , 99.95%) were supplied by the El-Nasr pharmaceutical chemicals company (Egypt). Bi-distilled water was used as a solvent and/or adsorption media. The prepared  $\text{SiO}_2$  nanostructures were characterized by X-ray diffraction

(XRD), Fourier transform infrared spectroscopy (FT-IR), field-emission scanning electron microscope (FE-SEM), and transmission electron microscope (TEM).

### 2.2 Preparation of $\text{SiO}_2$ Nanoparticles

Silicon dioxide ( $\text{SiO}_2$ ) was prepared by a simple and direct sol–gel method. In a typical synthesis process: 4.0 g of silica gel was dissolved in an aqueous solution of  $\text{NaOH}$  (2 M, 30 mL) with a continuous stirring for 40 min and heating at 70 °C. The produced solution was allowed to get the room temperature then an aqueous solution of 2 M  $\text{HNO}_3$  was added drop wise so as to attain a specific pH (6, 7, and 8), yielding a colorless gel. The obtained gel was allowed to stir for two hours. The produced gel was washed with bi-distilled water several times, via centrifugation, to remove the impurities (sodium hydroxide and sodium nitrate). The produced white products were dried at 120 °C for 4 h. Finally, the produced powders were calcined at 800 °C for 2 h, generating fine white powder. The white powder obtained at pH values of 6, 7 and 8 were referred to as  $S_1$ ,  $S_2$  and  $S_3$ , respectively.

### 2.3 Adsorption Studies

The adsorption performance of the as-prepared silicon dioxide nanostructure was evaluated for Cd(II) and Pb(II) ions removal through batch adsorption experiments with various parameters including pH, initial concentration, dose of the adsorbent, contact time and temperature. Cd(II) and Pb(II) concentrations were analyzed by atomic absorption spectrometer and each sample was measured in triplicate, and the average results are reported [41]. The removal efficiency ( $R, \%$ ) and adsorption capacity ( $q_e, \text{mg g}^{-1}$ ) of the silicon dioxide adsorbent were calculated using the following equations:

$$\text{Adsorption efficiency}(R, \%) = (C_0 - C_e)/C_0 \times 100 \quad (1)$$

$$\text{Adsorption capacity}(q_e, \text{mg g}^{-1}) = [(C_0 - C_e)V]/m \quad (2)$$

where  $q_e$  is equilibrium adsorption capacity of silicon dioxide adsorbent toward the selected ions ( $\text{mg g}^{-1}$ ),  $C_0$  and  $C_e$  are the initial and equilibrium concentrations of the selected ions in the solution ( $\text{mg/L}$ ), respectively,  $V$  is the volume of the solution (L), and  $m$  is the weight of adsorbent (g).

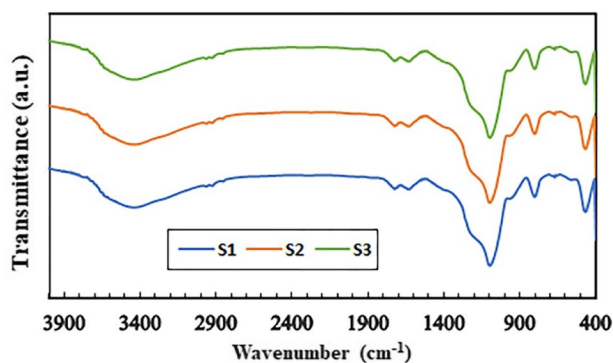


**Fig. 1** FT-IR spectra of the prepared silicon dioxide nanoparticles ( $S_1$ ,  $S_2$  and  $S_3$  samples) before calcination

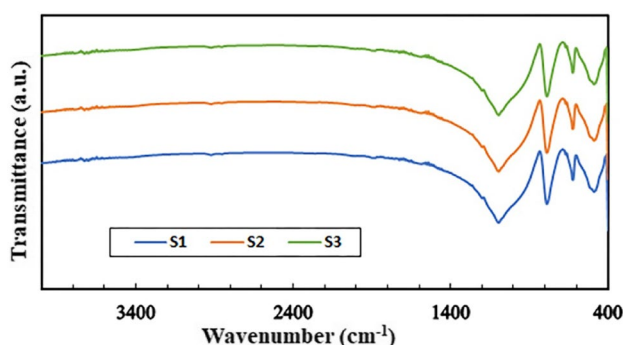


**Fig. 2** FT-IR spectra of the prepared silicon dioxide nanoparticles ( $S_1$ ,  $S_2$  and  $S_3$  samples) after calcination at 800 °C for 2 h

## 3 Results and Discussion

### 3.1 Characterization of the Synthesized $\text{SiO}_2$ Nano-adsorbent

#### 3.1.1 FT-IR Spectra Analysis

The infrared spectra of the as-prepared  $\text{SiO}_2$  nanoparticles ( $S_1$ ,  $S_2$  and  $S_3$ ) before and after calcination are shown in Figs. 1 and 2, respectively. Figure 1 revealed that  $S_1$ ,  $S_2$  and  $S_3$  samples without calcination have similar spectra. These samples showed absorption bands at 1630 and 3440  $\text{cm}^{-1}$  ascribed to the stretching and bending of the adsorbed water molecules on the surface of the synthesized silicon dioxide [30]. Besides, two bands appeared at around 1200 and 1090  $\text{cm}^{-1}$  are related to the asymmetric and symmetric vibrational modes of the Si–O–Si bands. Two bands appeared at ca. 795 and 460  $\text{cm}^{-1}$  are assigned to symmetric stretching and tetrahedral bending of Si–O bonds, respectively. These typical bands are assigned to the formation of silicon dioxide nanoparticles. On the

other hand, after calcination at 800 °C for 2 h (Fig. 2), three dominant bands were observed at ca. 488, 788 and 1094  $\text{cm}^{-1}$  which can be attributed to the bending vibrations of Si–O, symmetric stretching vibrations of O–Si–O, and asymmetric vibrations of Si–O–Si, respectively [30]. The results indicated that calcination resulted in disappearance of the vibrational bands of the Si–OH groups and surface adsorbed water molecules of the  $\text{SiO}_2$  samples [30, 42, 43].

#### 3.1.2 XRD Studies

From Fig. 3, the diffraction peaks of ( $S_1$ ) sample calcined at 800 °C can be indexed to a mixture of tridymite phase (50%, JCPDS No. 00-003-0218) and cristobalite phase (50%, JCPDS No. 00-002-0278). While the diffraction peaks of ( $S_2$ ) sample calcined at 800 °C can be indexed to a mixture of quartz phase (JCPDS No. 00-013-0026) and low- $\alpha$  quartz phase (JCPDS No. 00-005-0490). Finally, the diffraction peaks of ( $S_3$ ) sample calcined at 800 °C can be indexed to a mixture of cristobalite alpha phase (JCPDS No. 00-003-0271) and quartz-beta phase (JCPDS No. 00-007-0346) [30]. The average crystallite sizes of the calcined products were estimated using the following Debye–Scherrer equation, Eq. (3) [44]:

$$D = 0.9\lambda / \beta \cos \theta_B \quad (3)$$

where  $\lambda$ ,  $\theta_B$  and  $\beta$  are the X-ray wavelength, Bragg diffraction angle, and the XRD pattern peaks full width at half maximum (FWHM), respectively. The results revealed that the average crystallite size values for  $S_1$ ,  $S_2$  and  $S_3$  samples calcined at 800 °C were found to be ca. 37.7, 40.0 and 45.2 nm, respectively. Since  $S_1$  sample has the smallest crystallite size, it has been chosen for the subsequent experiments.

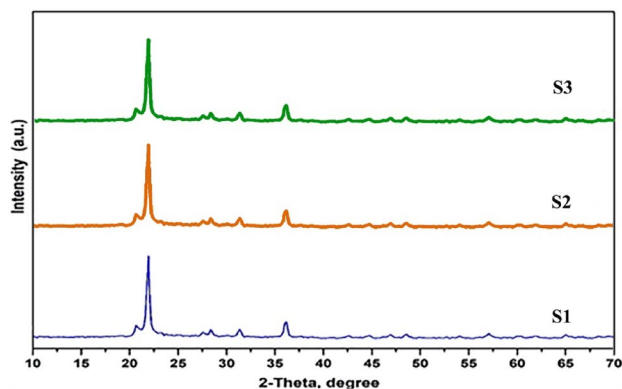


**Fig. 3** XRD patterns of the as-prepared silicon dioxide nanoparticles ( $S_1$ ,  $S_2$  and  $S_3$  samples) after calcination at 800 °C for 2 h

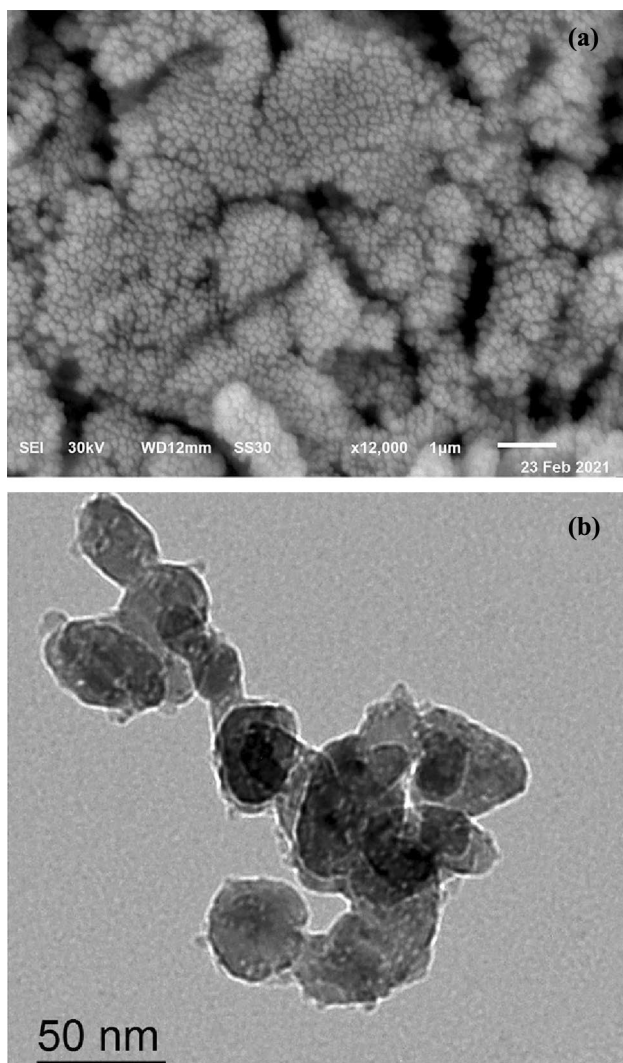


Fig. 4 FE-SEM (a) and TEM (b) images of  $S_1$  sample

### 3.1.3 Morphology Studies

The morphology of the as-prepared silicon dioxide nanoparticles ( $S_1$  sample) was characterized by FE-SEM and HR-TEM as displayed in Fig. 4. FE-SEM images of the  $SiO_2$  sample displayed that the fabricated silicon dioxide product consisted of porous aggregates of spherical shaped particles as shown in Fig. 4a. Besides, the microstructure of the  $SiO_2$  product was investigated using TEM as shown in Fig. 4b. The TEM image revealed that the  $SiO_2$  product ( $S_1$ ) is composed of spherical and irregular particles of an average particle size of ca. size ca. 38 nm. These results are compatible with the XRD data.

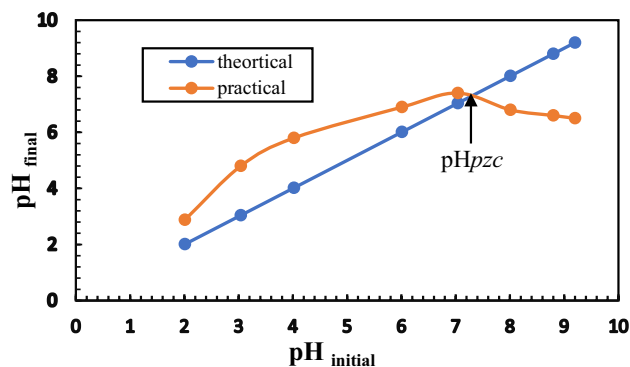


Fig. 5 Point of zero charge ( $pH_{pzc}$ ) of mesoporous silicon dioxide ( $S_1$ )

## 3.2 Adsorption Studies

### 3.2.1 $pH_{pzc}$ Determination

The  $pH_{pzc}$  (point of zero charge) is the pH value at which the net surface charge of the  $SiO_2$  particles equals zero. It is an important parameter elucidating the adsorption mechanism of sorbed species at the surface. At pH value lower than that of  $pH_{pzc}$ , the net surface charge of the adsorbent is positive which results in an electrostatic repulsion between the positively charged  $SiO_2$  particles and the cationic species, and possibly inhibit the adsorption of such species from aqueous solutions. On the other hand, at pH higher values, the surface charge of adsorbent possesses a net negative charge due to the acidic dissociation of  $H^+$  ions from the surface  $Si-OH$  groups, and the produced negatively charged particles favor the uptake of positively charged species (in the present case  $Pb(II)$  and  $Cd(II)$ ). The point of zero charge ( $pH_{pzc}$ ) of  $SiO_2$  nanoparticles ( $S_1$ ) was estimated using the pH drift method [45]. As such, suspensions of  $SiO_2$  in 0.01 M solutions of NaCl with different initial pH values (2.0–9.2) were used for this estimation. The initial pH values ( $pH_{initial}$ ) were plotted against the final pH values ( $pH_{final}$ ) (Fig. 5), and the point of intersection between the  $pH_{initial}$ – $pH_{final}$  curve and the  $pH_{initial} = pH_{final}$  line marks the  $pH_{pzc}$  value. The  $pH_{pzc}$  value of the  $S_1$  adsorbent was found to be around 7.2, consequently, it is preferred to remove cations at  $pH > 7.2$  to ensure that the net surface of  $S_1$  being negative.

### 3.2.2 Adsorption Properties of the Prepared $SiO_2$ Nanoparticles

Adsorption is an efficient and economically feasible process for the wastewater containing chemically stable pollutants such as heavy metals. We investigated the adsorption

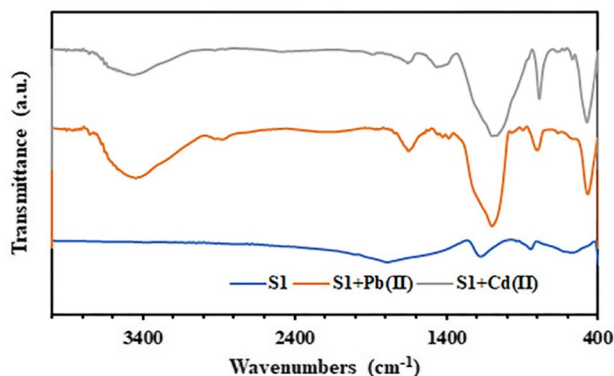


**Fig. 6** FT-IR spectra for  $S_1$  adsorbent before and after adsorption

properties of the as-prepared  $SiO_2$  nanoparticles for  $Pb(II)$  and  $Cd(II)$  ions as a toxic pollutant. Adsorption capacity represents one of the more characteristics features to decide which sample is more convenient for heavy metal removal processing. The FT-IR spectra can be used as an evidence for the adsorption process of heavy metals [41, 46]. Figure 6 depicts the FT-IR spectra of the prepared adsorbent before and after adsorption of  $Pb(II)$  and  $Cd(II)$  ions. From Fig. 6, it is observed that the spectrum of  $Pb(II)$  and  $Cd(II)$  metal-loaded for  $S_1$  differs from that adsorbent before the adsorption. The difference between the FT-IR spectra of the prepared adsorbents before and after adsorption in all spectrum is probably due to the adsorbed  $Pb(II)$  and  $Cd(II)$  ions onto the adsorbent.

**3.2.2.1 Effect of pH** The solution pH is considered one of the most effective and crucial parameters in the adsorption of heavy metals because it can both affect the surface charge properties of the adsorbent and the aqueous distribution of metal ions. Therefore, adsorption of  $Cd(II)$  and  $Pb(II)$  ions on the surface of as-prepared silicon dioxide was studied in the pH range of 2.5–9.0 which was adjusted by using HCl and NaOH (0.2 M) with an adsorbent dosage of 0.05 g and initial  $Cd(II)$  and  $Pb(II)$  ions concentration of 50 mg/L at 298 K. The adsorption progress by protonation and deprotonation of adsorbent surface functional groups are influenced by the pH of the adsorption media. The pH of the solution controls the adsorption behavior of the metal ions onto the adsorbent particles. It also affects the solubility of the metal ions in the solution, replaces some of the positive ions found in the active sites, and affects the degree of ionization of the adsorbate during the reaction. The effect of initial pH on the sorption of  $Pb(II)$  ions onto the utilized nanoparticles was evaluated within the pH range of 2.5–9.0. The metal removal from solution at pH beyond 10 would not give accurate results because precipitation of the ions as hydroxides took place. This was the reason why the removal curve became high as there were not lead ions to be removed

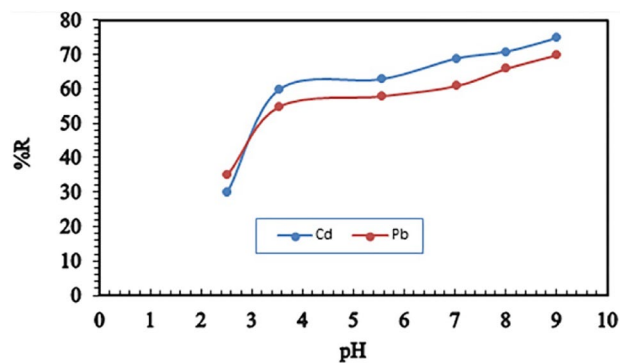


**Fig. 7** Effect of pH on the efficiency of removing  $Cd(II)$  and  $Pb(II)$  ions using the as-prepared  $SiO_2$  nanoparticles

(the solution seems to be clear because of the metal precipitation) at these pH values. The effect of different pH values ranged from 2.5 to 9.0 on the adsorption of  $Pb(II)$  and  $Cd(II)$  ions by  $SiO_2$  ( $S_1$ ) nanoparticles (1 g/L) for 24 h contact time was investigated and displayed in Fig. 7. The initial concentration of  $Pb(II)$  and  $Cd(II)$  ions, adsorbent dose, volume of metal ions and stirring rate were set at 50 ppm, 0.05 g, 50 mL, and 400 rpm, respectively, at 298 K for 24 h.

The effect of pH on the adsorption behavior of  $SiO_2$  for  $Pb(II)$  and  $Cd(II)$  ions were shown in Fig. 7. It can be seen that at lower pH values, the surface of adsorbent has a positive charge, and therefore lower pH values are not favored for adsorption of  $Cd(II)$  and  $Pb(II)$ . Besides, the presence of excess  $H^+$  ions in the solution competing with the positive  $Cd(II)$  and  $Pb(II)$  ions is another result for the low adsorption efficiency at lower pH values (i.e. pH 2.5) [47]. As the pH value was raised, the number of negatively charged adsorption sites, generated by the deprotonation of functional groups on silicon dioxide ( $S_1$ ) adsorbent, increased. Therefore, the high electrostatic attraction between these

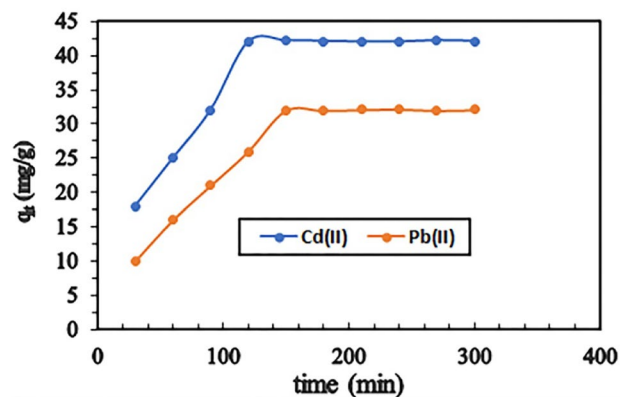


**Fig. 8** Effect of adsorption time on the adsorption capacity of  $SiO_2$  for removing  $Cd(II)$  and  $Pb(II)$  ions

negatively charged surface of the adsorbent and positively charged Cd(II) and Pb(II) ions enhanced the adsorption efficiency [48]. Consequently, pH 9 was considered suitable value for the effective removal of Cd(II) and Pb(II) ions by ( $S_1$ ) adsorbent.

**3.2.2.2 Adsorption Contact Time** As shown in Fig. 8, the adsorption contact time has a significant influence on the efficiency of removing Cd(II) and Pb(II) ions under following conditions: 50 mg/L of initial concentration of Cd(II) and Pb(II) ions, 1 g/L of the prepared silicon dioxide ( $S_1$ ) nanoparticles, room temperature, and pH 9. The results showed that with increasing the contact time from 30 to 120 min the adsorption capacity reached ca.  $42.2 \text{ mg g}^{-1}$  for Cd(II) ions. And with increasing the contact time from 30 to 150 min the adsorption capacity reached ca.  $32.2 \text{ mg g}^{-1}$  for Pb(II) ions. Afterwards the adsorption processes reached their equilibrium for both ions. Overall, each adsorption process can be divided into three stages. The three states are described as follows: Firstly, at the beginning of adsorption, the adsorption efficiency increased dramatically because the adsorption occurs mainly on the surface of adsorbent. Then, at the second stage, the increasing efficiency of adsorption became slow and this is probably due to the decrease in Cd(II) and Pb(II) ion concentration in solution. The other reason is that during this stage the adsorption works mainly in the internal surface of adsorbent pores to decrease the mass transfer rate. Finally, the adsorption reaches an equilibrium state when the Cd(II) and Pb(II) ions residue is much less. These results are in accordance with that of the adsorption of some cations on some porous materials [49]. Based on the obtained results, the adsorption efficiencies increased their highest values; 68% for Pb(II) ions in 120 min and 80.2% for Cd(II) ions in 150 min. Accordingly, the adsorption contact time was set as 120 min and 150 min for Cd(II) and Pb(II) ions, respectively, in the following adsorption studies.

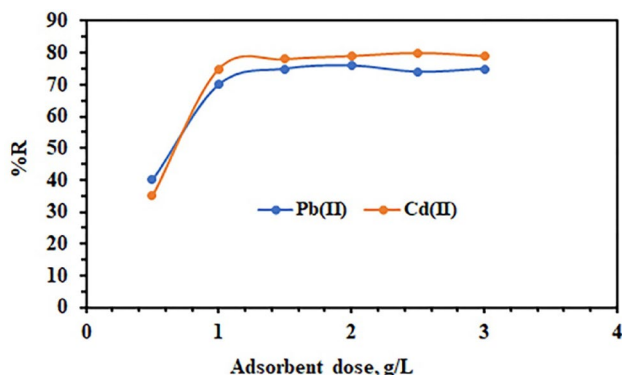


**Fig. 9** Effect of adsorbent dose on the efficiency of removing Cd(II) and Pb(II) ions

**3.2.2.3 Adsorbent Dose** Figure 9 shows the effect of the dosage (0.5–3 g/L) of ( $S_1$ ) sample on the efficiency of removing Cd(II) and Pb(II) ions under following conditions: 50 mg/L of initial concentration of Cd(II) and Pb(II) ions, (0.5–3 g/L) dose of the prepared silicon dioxide ( $S_1$ ) nanoparticles, room temperature, and pH 9, after 120 and 150 min. As shown in Fig. 9, the removal efficiency of Cd(II) and Pb(II) ions was increased from 35 to 93% and 40 to 92% as the dose of ( $S_1$ ) sample increased from 0.5 to 3 g/L. The significant enhancement in adsorption capacities can be due to the high accessibility of larger number of adsorption sites due to the increasing in the dose of  $S_1$  [49]. However, at higher dosage of the adsorbent, some agglomerations occurred. Therefore, 1 g/L ( $S_1$ ) dose was selected for the subsequent experiments.

**3.2.2.4 Initial Metals Concentration** Under conditions: 1 g/L ( $S_1$ ) dosage, pH 9, adsorption time 120 min for Cd(II) and 150 min for Pb(II), and room temperature, the effect of Cd(II) and Pb(II) initial concentrations on the removal efficiency was carried out. It could be observed from Fig. 10 that the adsorption efficiency decreased while the initial concentrations of Cd(II) and Pb(II) ions increased. Obviously, the adsorption efficiency reached the optimum values of 89% and 91% for Cd(II) and Pb(II) ions, respectively, at an initial ion concentration 10 mg/L for both cations. The results may be interpreted as following. Firstly, the adsorption quantity of the ions on the adsorbent will be constant when a given mass of adsorbent is used. Then the amount of residual Cd(II) and Pb(II) ions can be increased as the initial concentrations raised, which can lead to reducing the removing efficiency [49]. In other words, the available adsorption sites reduced as the initial concentration of the cations of interest increased.

**3.2.2.5 Effect of Temperature** Temperature degree has an essential role affect on the rate of adsorption process. The

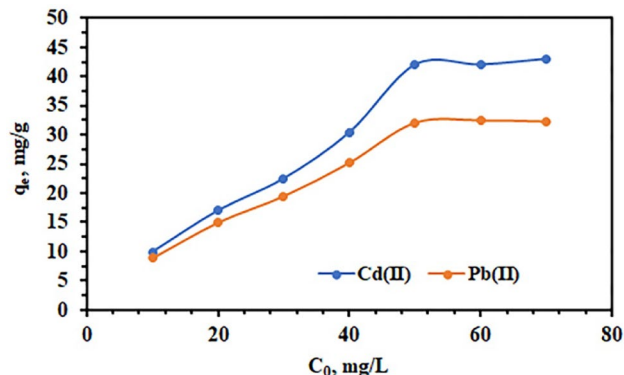


**Fig. 10** Effect of initial concentration of Cd(II) and Pb(II) ions on their adsorption on  $\text{SiO}_2$  nanoparticles

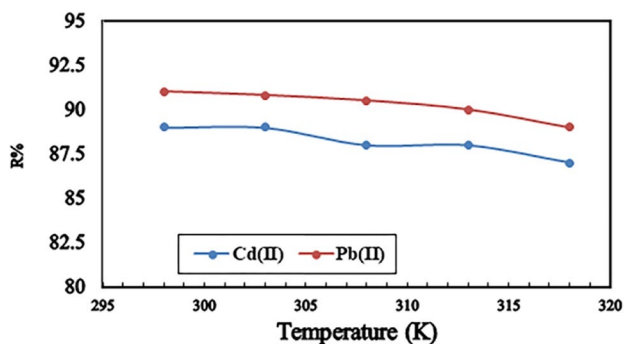


**Fig. 11** Effect of temperature on Cd(II) and Pb(II) removal percent using SiO<sub>2</sub> (S<sub>1</sub>) nanoparticles

adsorption studies were carried out at different temperatures (298, 303, 308, 313 and 318 K) separately for Cd(II) and Pb(II) ions using 0.05 g of (S<sub>1</sub>) nanoparticles at the obtained optimum conditions as illustrated in Fig. 11. The experimental results showed that the adsorption capacity decreased slowly with increasing the solution temperature as shown in Fig. 11. This indicates that the adsorption of metal ions on the prepared adsorbents is an exothermic process. The decrease in the rate of adsorption with the increase in temperature may be attributed to the tendency of metal ions to escape from the solid phase to bulk liquid phase at higher temperature values [49].

### 3.3 Adsorption Kinetic Study

Adsorption kinetic studies are necessary in the treatment of aqueous effluents because they provide valuable information on the mechanism of the adsorption process which is crucial for the practicality of the process. The mechanism of the adsorption process depends on the physical and chemical characteristics of the adsorbent and adsorbate. The mechanism and rate of adsorption were proposed by fitting the experimental kinetic data to pseudo-first-order ( $\log(q_e - q_t)$  and  $t$ ) and pseudo-second-order ( $t/q_t$  and time  $t$ ) models [50] as represented in Eqs. (4), (5).

$$\log(q_e - q_t) = \log q_e - k_1/2.303t \tag{4}$$

where  $q_e$  and  $q_t$  are the amount of heavy metal ions adsorbed on the adsorbent in mg (metal)/g (adsorbent) at equilibrium and at time  $t$ , respectively.  $k_1$  is the rate constant of first-order kinetics in  $\text{min}^{-1}$ . While the pseudo-second-order kinetic model can be written as given in Eq. (5).

$$t/q_t = 1/k_2q_e^2 + t/q_e \tag{5}$$

where  $q_e$  and  $q_t$  are the amount of heavy metal ions adsorbed by the adsorbent in mg (metal)/g (adsorbent) at equilibrium

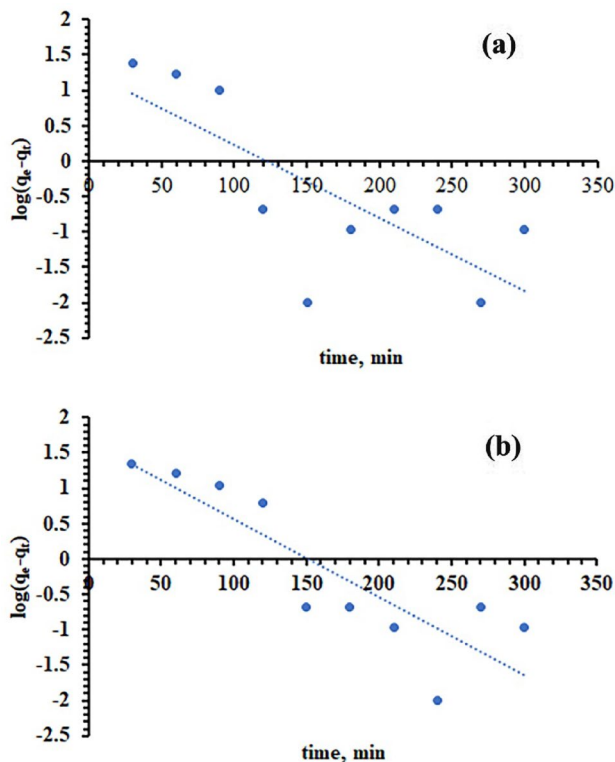


**Fig. 12** Pseudo-first-order plots for adsorption of **a** Cd(II) and **b** Pb(II) ions onto SiO<sub>2</sub> (S<sub>1</sub>) nanoparticles

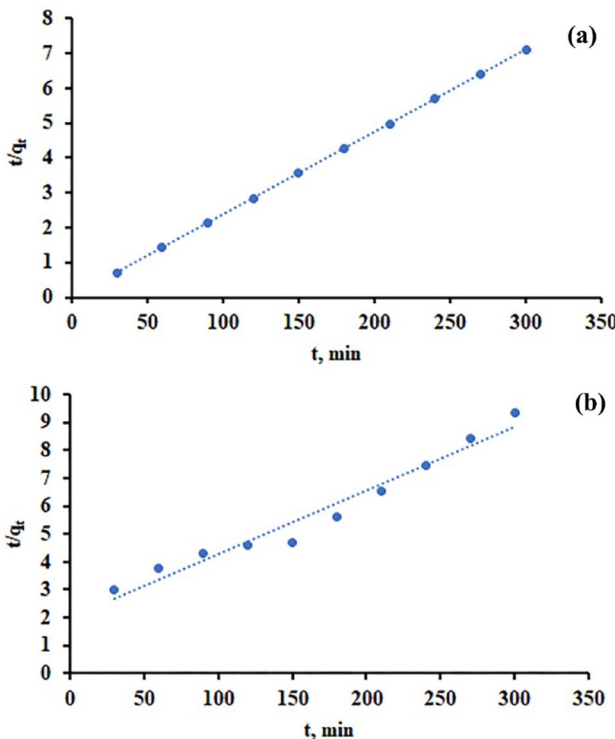


**Fig. 13** Pseudo-second-order plots for adsorption of **a** Cd(II) and **b** Pb(II) onto (S<sub>1</sub>) nanoparticles

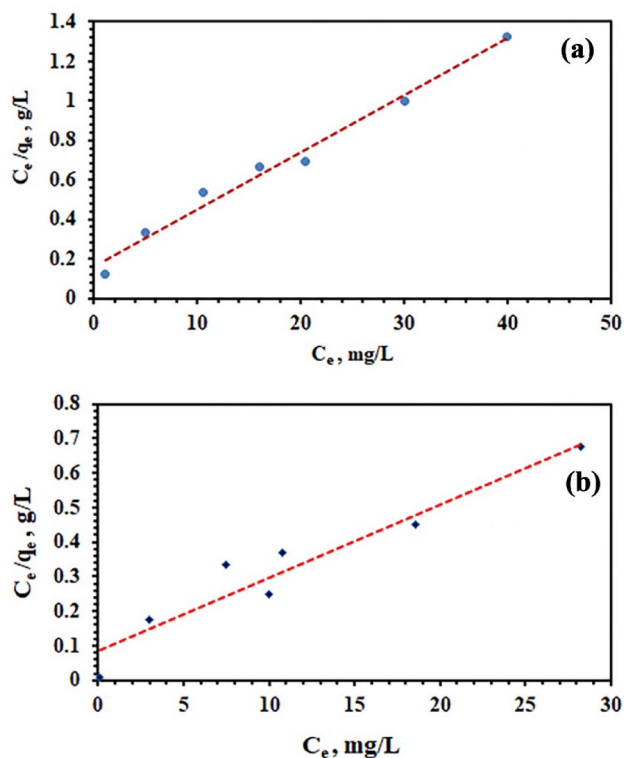
**Table 1** Kinetic parameters for the adsorption of Cd(II) and Pb(II) ions onto SiO<sub>2</sub> (S<sub>1</sub>) nano-adsorbent

Kinetics models	Constants	Values	
		Pb(II)	Cd(II)
Pseudo-first-order	$k_1$ (1/min)	0.0252	0.0236
	$q_{e(cal)}$ (mg/g)	45.38	18.699
	$r_1^2$	0.7534	0.5736
	$q_{e(exp)}$ (mg/g) at $C_0=50$ mg/L	32.2	42.2
Pseudo-second-order	$k_2$ [g/(mg min)]	0.00026	0.00044
	$q_{e(cal)}$ (mg/g)	44.01	50.11
	$r_2^2$	0.963	0.9813
	$q_{e(exp)}$ (mg/g) at $C_0=50$ mg/L	32.2	42.2

and at time  $t$ , respectively.  $k_2$  is the rate constant of second-order kinetics in g/(mg/min). The values of  $k_1$  and  $k_2$  were determined from Eqs. (4) and (5), respectively [51]. Figures 12 and 13 display the results of the kinetic relations for the removal of lead and cadmium ions. The parameters of pseudo-first-order model and pseudo-second-order model for the adsorption of Pb(II) and Cd(II) on S<sub>1</sub> nanoparticles are tabulated in Table 1. According to the values of  $R^2$  for the examined experimental data using various models, the pseudo-second-order model is the better fitting ( $R^2=0.995$ ) than the pseudo-first order ( $R^2=0.778$ ) for the removal of the lead ions. And the values of  $R^2$  for the tested experimental data exhibited that the pseudo-second-order model is the better fitting ( $R^2=0.993$ ) than the pseudo-first order ( $R^2=0.523$ ) for the removal of the cadmium ions. So, we can say that the adsorption of cadmium and lead ions from aqueous solution onto (S<sub>1</sub>) followed the pseudo-second-order model.

### 3.4 Isotherm Studies

The common isotherm models (Langmuir and Freundlich) were used to describe the adsorption of Pb(II) and Cd(II) ions on the nanoparticles. Langmuir model supposed that all the adsorption sites of the adsorbent have the same binding energy and every site joints to only one adsorbate ion/molecule [51, 52]. This model of isotherm assumes the formation of a monolayer adsorbate on the outer surface of the adsorbent, and after that no further adsorption takes place. It is valid for monolayer adsorption onto a surface containing a finite number of identical sites. It assumes uniform energies of adsorption onto the surface and no transmigration of adsorbate in the plane of the surface. The linearized Langmuir isotherm form is given by Eq. (6):

**Fig. 14** Langmuir isotherm model for a Pb(II) and b Cd(II) adsorption onto (S<sub>1</sub>) nanoparticles

$$\frac{C_e}{q_e} = \frac{b}{q_m} + \frac{1}{q_m} C_e \quad (6)$$

where  $q_e$  is the equilibrium adsorption capacity of the adsorbent in mg (metal)/g (adsorbent),  $C_e$  is the equilibrium concentration of metal ions in (mg/L),  $q_m$  is the maximum adsorption capacity of the adsorbent in mg(metal)/g(adsorbent), and  $b$  is the Langmuir constant that belongs to the bonding energy of adsorption in (L/mg). Linear plot of  $C_e/q_e$  versus  $C_e$  shows Langmuir isotherm (Fig. 14), the obtained values of  $q_m$  and  $b$  were calculated from the slope and intercept of the linear plots (Table 2). The essential characteristics of Langmuir isotherm can be expressed by a dimensionless constant called equilibrium parameters,  $R_L$ , defined in Eq. (7):

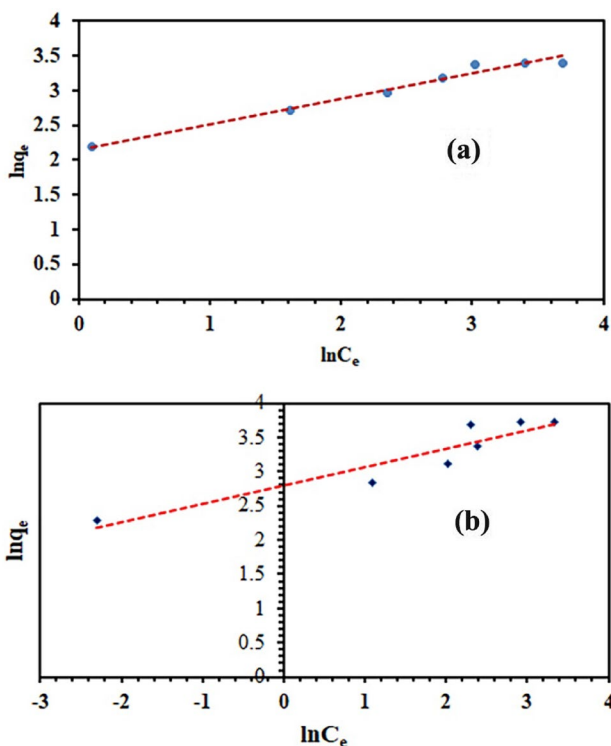
$$R_L = \frac{1}{1 + bC_0} \quad (7)$$

where  $b$  is the Langmuir constant and  $C_0$  is the initial metal ion concentration (mg/L), and  $R_L$  value indicates the adsorption nature to be either: unfavorable if  $R_L > 1$ , Linear if  $R_L = 1$ , favorable if  $0 < R_L < 1$  and irreversible if  $R_L = 0$  [51, 52]. The obtained  $R_L$  values were between zero and one, which indicate favorable adsorption.



**Table 2** Constants of the Langmuir and Freundlich isotherms for the adsorption of Pb(II) and Cd(II) ions on SiO<sub>2</sub> (S<sub>1</sub>) nano-adsorbent

Adsorption isotherm model	Parameters	Values	
		Pb(II)	Cd(II)
Langmuir	K <sub>L</sub> (L/mg)	0.1779	0.2425
	q <sub>m(cal)</sub> (mg/g)	34.67	47.29
	r <sub>1</sub> <sup>2</sup>	0.982	0.921
	R <sub>L</sub>	0.0669–0.3342	0.0669–0.3342
	q <sub>e(exp)</sub> (mg/g) at C <sub>0</sub> = 50 mg/L	32.2	42.2
Freundlich	K <sub>F</sub> [(mg/g) (L/mg) <sup>1/n</sup> ]	8.579	16.46
	q <sub>m(cal)</sub> (mg/g)	68.92	68.12
	r <sub>2</sub> <sup>2</sup>	0.977	0.870
	n	2.737	3.731
	q <sub>e,(exp)</sub> (mg/g) at C <sub>0</sub> = 50 mg/L	32.2	42.2

**Fig. 15** Freundlich isotherm for **a** Pb(II) and **b** for Cd(II) adsorption on (S<sub>1</sub>) nanoparticles

On the other hand, Freundlich isotherm model is used to describe the adsorption characteristics for the heterogeneous surface [51, 52]. It assumes heterogeneity of binding energies of adsorption sites. The linearized Freundlich isotherm form is given by Eq. (8).

$$\ln q_e = \ln K_f + \left(\frac{1}{n}\right) \ln C_e \quad (8)$$

where  $q_e$  is the equilibrium adsorption capacity of the adsorbent in mg/g,  $C_e$  is the equilibrium concentration of heavy metal ions in (mg/L),  $K_f$  is the constant refers to the

adsorption intensity of the adsorbent in [(mg/g)(L/mg)<sup>1/n</sup>], and  $n$  is the constant linked to the adsorption intensity.  $(1/n)$  is the heterogeneity factor and it is a function of the strength of adsorption in the adsorption process [51, 52]. If  $n = 1$  (i.e.  $(1/n) = 1$ ), the partition between the two phases are independent of the concentration. If value of  $1/n$  is below one, it indicates a normal adsorption. If  $1/n$  is above one, it indicates a cooperative adsorption [51, 52]. In addition, if  $n$  lies between one and ten, this indicates a favorable sorption process [51, 52]. According to Freundlich isotherm model,  $\ln q_e$  is plotted against  $\ln C_e$  and the data are treated by linear regression analysis, as shown in Fig. 15 for metal ion adsorption on S<sub>1</sub>.  $1/n$  and  $K_f$  constants are determined from the slope and intercept of the plots. Based on the tabulated values of  $1/n$  and  $n$  in Table 2, it can be concluded that the sorption of Pb(II) and Cd(II) ions onto the prepared nano-sized SiO<sub>2</sub> particles is favorable. The constants of the Langmuir and Freundlich isotherm models are presented in Table 2. Although, we determined the maximum adsorption capacity ( $q_m$ ) by using the Langmuir model, this value can be also calculated from the Freundlich isotherm model by using Eq. (9) [53].

$$K_f = \frac{q_m}{C_0^{1/n}} \quad (9)$$

According to the listed data in Table 2, it can be concluded that the experimental data can be described well using the Langmuir isotherm model because the higher  $r^2$  values and closer calculated maximum adsorption capacity;  $q_m$  ( $q_{m(cal)}$ ), to the experimental  $q_m$  ( $q_{m(exp)}$ ) obtained from this model compared to those obtained from the Freundlich isotherm model. Consequently, the adsorption of the cations of interest may take place through a monlayer adsorption and homogeneously distributed on the active sites of the surface of the as-prepared adsorbent.

### 3.5 Thermodynamic Studies

The effect of adsorption media temperatures on the adsorption of the ions of interest on the as-prepared adsorbent was explored in the range of 298–318 K, as shown previously in Fig. 11, under the adsorption conditions: 0.05 g adsorbent, 50 mg/L initial concentration of the metal ion, and 400 rpm stirring rate. The results exhibited that the decrease in the rate of adsorption with the increase of the temperature can be attributed to the low tendency of Pb(II) and Cd(II) ions to the solid phase at higher temperatures. The values of thermodynamic parameters such as change in enthalpy ( $\Delta H^\circ$ ), change in entropy ( $\Delta S^\circ$ ), and change in Gibbs free energy ( $\Delta G^\circ$ ), were determined by using the following Eq. (10) [54]:

$$\ln K_c = (\Delta S^\circ/R) - (\Delta H^\circ/RT) \quad (10)$$

where  $K_c = C_{Ac}/C_c$ .  $K_c$  is the equilibrium constant,  $C_{Ac}$  is the solid phase concentration at equilibrium (mg/L),  $T$  is the temperature in Kelvin, and  $R$  is the gas constant. By plotting  $\ln K_c$  against  $1/T$  gives a straight line with a slope and intercept equal to  $(-\Delta H^\circ/R)$  and  $\Delta S^\circ/R$ , respectively. The values of  $\Delta H^\circ$  and  $\Delta S^\circ/R$  were calculated from Fig. 16a, b

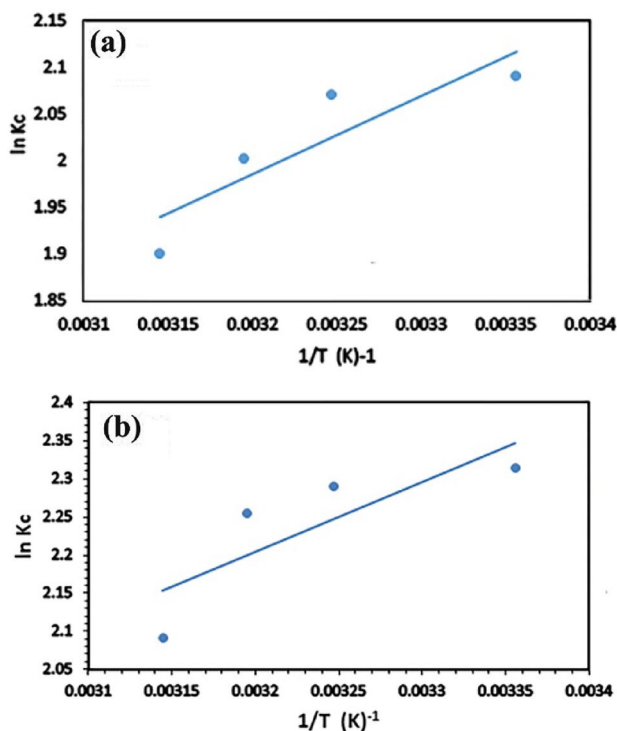


**Fig. 16** Plots of  $\ln K_c$  against  $1/T$  for **a** Cd(II) and **b** Pb(II) adsorption on ( $S_1$ ) nanoparticles

**Table 3** Thermodynamic parameters for the adsorption of Pb(II) and Cd(II) on  $S_1$  nanoparticles

Adsorbate	Temperature (K)	$\ln K_c$	$\Delta G^\circ$ (kJ/mol)	$\Delta H^\circ$ (kJ/mol)	$\Delta S^\circ$ (kJ/mol k)
Cd(II)	298	2.091	-5.1799		
	308	2.07	-5.3019	-7.003	0.0059
	313	2.002	-5.2096		
	318	1.901	-5.0259		
Pb(II)	298	2.314	-5.7322		
	308	2.289	-5.8626	-7.607	0.006
	313	2.254	-5.8657		
	318	2.091	-5.5276		

and reported in Table 3. The negative values of  $\Delta H^\circ$  indicate the exothermic nature of the adsorption process of Cd(II) and Pb(II) on the  $S_1$  product. The positive values of entropy changes,  $\Delta S^\circ$ , correspond to an increase in degree of freedom of the adsorbed species. Gibbs free energy change,  $\Delta G^\circ$ , of the adsorption process was calculated from Eq. (11) and the values are given in Table 3.

$$(\Delta G^\circ) = \Delta H^\circ - T\Delta S^\circ \quad (11)$$

The negative values of ( $\Delta G^\circ$ ) indicated that the adsorption of both metal ions on  $S_1$  product is a spontaneous process and the decrease in ( $\Delta G^\circ$ ) values with increasing the temperature indicates that the adsorption process is less preferable at higher temperature values. The negative value of  $\Delta H^\circ$  indicates that the adsorption process is exothermic.

**Table 4** Comparison study between current work and literature studies for the adsorption of Pb(II) and Cd(II) ions on different adsorbents

Adsorbate	Adsorbent	Adsorption capacity (mg/g)	References
Pb(II)	Zero-valent iron	90.10	[55]
Pb(II)	Polymer based graphene oxide	73.52	[56]
Pb(II)	Nano-sized silicon oxide	34.2	This work
Cd(II)	Alumina nanoparticles	0.608	[57]
Cd(II)	Carbon nanotubes	181.8	[58]
Cd(II)	Nano-sized silicon oxide	42.2	This work

### 3.6 Regeneration and Reproducibility

The results revealed that 0.4 M of EDTA di-sodium salt is a good media for the desorption of Cd(II) and Pb(II) ions from the prepared SiO<sub>2</sub> (S<sub>1</sub>) nanoparticles. In aqueous solution, EDTA is a hexadentate ligand that forms highly stable complexes with Cd(II) and Pb(II) ions. As a result, it has an affinity for taking off the adsorbed metal ions from the surface of the prepared SiO<sub>2</sub> (S<sub>1</sub>) nanoparticles. In terms of time and money, it's better to choose adsorbent materials that can be reused multiple times without losing their effectiveness. There is no deterioration in the percent of removing or the adsorption capacity of the synthesized SiO<sub>2</sub> (S<sub>1</sub>) nanoparticles after four adsorption cycles. Thus as a result, these the prepared SiO<sub>2</sub> (S<sub>1</sub>) nanoparticles are effective, reusable, and stable, and they may be utilized repeatedly without losing their efficiency against cadmium and lead ions.

### 3.7 Comparison Study

The produced SiO<sub>2</sub> nanoparticles' adsorption capabilities for lead and cadmium ions were compared to those of other adsorbents and listed in Table 4. In addition, Table 4 displays that the as-prepared SiO<sub>2</sub> (S<sub>1</sub>) nanoparticles have a maximum adsorption capacity (q<sub>m</sub>) of ca. 32.2 and 42.2 mg g<sup>-1</sup> for the removal of lead and cadmium ions from aqueous media which are relatively higher than those published for other adsorbents toward the cations of interest. Therefore, the as-prepared SiO<sub>2</sub> (S<sub>1</sub>) nanoparticles can be considered as a promising candidate for the removal of Cd(II) and Pb(II) ions from aqueous media. This is due to the relatively high efficiency of the as-prepared SiO<sub>2</sub> nano-adsorbent and its relatively long-term regeneration for the removal of Cd(II) and Pb(II) ions from aqueous solutions.

### 3.8 Application of the as-Prepared SiO<sub>2</sub> on Real Water Samples

The attained optimum conditions for the removal of Cd(II) and Pb(II) ions from aqueous solutions were applied on real water samples. It notable that as detailed in the experimental section, the produced nanoparticles were employed to treat wastewater that contains lead (2.2 mg/L) and cadmium (3.52 mg/L) and collected from a factory for galvanization in Mubark Industrial Zone, Quesna city, Egypt. These pollutants were totally removed from the wastewater using the fabricated nanoparticles after utilizing the as-prepared SiO<sub>2</sub> nano-adsorbent and applying the optimum conditions. Consequently, the as-synthesized SiO<sub>2</sub> (S<sub>1</sub>) nanoparticles can be considered as a promising candidate for the removal of cations of interest from aqueous solutions.

## 4 Conclusions

Silicon dioxide nanoparticles (S<sub>1</sub>) were successfully prepared using direct and simple sol–gel method. The as-prepared silicon dioxide products were characterized using Fourier transform infrared spectroscopy (FT-IR), X-Ray diffraction (XRD), scanning electron microscopy (SEM), and transmission electron microscopy (TEM). The highly porous nanosized silicon dioxide high removal ability toward Cd(II) and Pb(II) ions from aqueous media. The results revealed long-term use of the adsorbent, and its maximum adsorption capacity was found to be 32.2 mg g<sup>-1</sup> and 42.2 mg g<sup>-1</sup> for Pb(II) and Cd(II) ions, respectively. The kinetics and isotherm modelling studies showed that the experimental data fitted well with the pseudo-second-order and Langmuir isotherm models, respectively. The obtained thermodynamic adsorption results indicated that the adsorption process of interest has spontaneous and exothermic natures. However, producing SiO<sub>2</sub> nanoparticles with smaller crystallite size is still challenging and it will be a useful point for our future direction.

**Acknowledgements** The second author (Mohamed S. Behiry) thanks A.A. Ali, Benha University, Egypt, for providing him some commercial chemicals.

### Declarations

**Conflict of interest** The authors declare that they have no conflict of interest.

**Informed Consent** Informed consent is not applicable to this study.

**Research Involving Human and/or Animal Participants** This article does not contain any studies with human participants or animals performed by any of the authors.

## References

1. S. Rajendran, T.A.K. Priya, K.S. Khoo, T.K.A. Hoang, H.-S. Ng, H.S.H. Munawaroh, C. Karaman, Y. Orooji, P.L. Show, A critical review on various remediation approaches for heavy metal contaminants removal from contaminated soils. *Chemosphere* **287**, 132369 (2022)
2. Z. Yan, Q. Zhao, M. Wen, L. Hu, X. Zhang, J. You, A novel polydentate ligand chromophore for simultaneously colorimetric detection of trace Ag<sup>+</sup> and Fe<sup>3+</sup>. *Spectrochim. Acta A* **186**, 17–22 (2017)
3. N. Zohora, D. Kumar, M. Yazdani, V.M. Rotello, R. Ramanathan, V. Bansal, Rapid colorimetric detection of mercury using bio-synthesized gold nanoparticles. *Colloids Surf. A* **532**, 451–457 (2017)
4. Y. Guo, Y. Sun, Z. Li, S. Feng, R. Yang, L. Qu, Detection, detoxification, and removal of multiply heavy metal ions using a recyclable probe enabled by click and declick chemistry. *J. Hazard. Mater.* **423**, 127242 (2022)

- M. Yap, N. Mubarak, J. Sahu, E. Abdullah, Microwave induced synthesis of magnetic biochar from agricultural biomass for removal of lead and cadmium from wastewater. *J. Ind. Eng. Chem.* **45**, 287–295 (2017)
- L.K. Wang, H. Yung-Tse, N.K. Shammass, Physicochemical treatment processes (2005)
- M.Y. Nassar, M.F. El-Shahat, A. Osman, M.M. Sobeih, M.A. Zaid, Adsorptive removal of manganese ions from polluted aqueous media by glauconite clay-functionalized chitosan nanocomposites. *J. Inorg. Organomet. Polym. Mater.* **31**, 4050–4064 (2021)
- M.Y. Nassar, I.S. Ahmed, Template-free hydrothermal derived cobalt oxide nanopowders: synthesis, characterization, and removal of organic dyes. *Mater. Res. Bull.* **47**, 2638–2645 (2012)
- M.Y. Nassar, E.I. Ali, E.S. Zakaria, Tunable auto-combustion preparation of TiO<sub>2</sub> nanostructures as efficient adsorbents for the removal of an anionic textile dye. *RSC Adv.* **7**, 8034–8050 (2017)
- Q. Chen, Y. Yao, X. Li, J. Lu, J. Zhou, Z. Huang, Comparison of heavy metal removals from aqueous solutions by chemical precipitation and characteristics of precipitates. *J. Water Process Eng.* **26**, 289–300 (2018)
- M.M. Matlock, B.S. Howerton, D.A. Atwood, Chemical precipitation of heavy metals from acid mine drainage. *Water Res.* **36**, 4757–4764 (2002)
- A. Bashir, L.A. Malik, S. Ahad, T. Manzoor, M.A. Bhat, G. Dar, A.H. Pandith, Removal of heavy metal ions from aqueous system by ion-exchange and biosorption methods. *Environ. Chem. Lett.* **17**, 729–754 (2019)
- Q. Dong, X. Guo, X. Huang, L. Liu, R. Tallon, B. Taylor, J. Chen, Selective removal of lead ions through capacitive deionization: role of ion-exchange membrane. *Chem. Eng. J.* **361**, 1535–1542 (2019)
- F.S. Awad, K.M. AbouZied, W.M. Abou El-Maaty, A.M. El-Wakil, M.S. El-Shall, Effective removal of mercury(II) from aqueous solutions by chemically modified graphene oxide nanosheets. *Arab. J. Chem.* **13**, 2659–2670 (2020)
- M. Kargar, G. Zolfaghari, Hybrid nano-filtration and micro-filtration pilot processes for the removal of chromium from water. *J. Water Wastewater* (2018). <https://doi.org/10.22093/wwj.2017.64518.2267>
- Z.T. Khanzada, Phosphorus removal from landfill leachate by microalgae. *Biotechnol. Rep.* **25**, e00419 (2020)
- R. Chen, Y. Cheng, P. Wang, Y. Wang, Q. Wang, Z. Yang, C. Tang, S. Xiang, S. Luo, S. Huang, C. Su, Facile synthesis of a sandwiched Ti<sub>3</sub>C<sub>2</sub>T<sub>x</sub> MXene/nZVI/fungal hypha nanofiber hybrid membrane for enhanced removal of Be(II) from Be(NH<sub>2</sub>)<sub>2</sub> complexing solutions. *Chem. Eng. J.* **421**, 129682 (2021)
- X. Zhang, X. Sun, T. Lv, L. Weng, M. Chi, J. Shi, S. Zhang, Preparation of PI porous fiber membrane for recovering oil-paper insulation structure. *J. Mater. Sci.: Mater. Electron.* **31**, 13344–13351 (2020)
- N.C.L. de Beluci, G.A.P. Mateus, C.S. Miyashiro, N.C. Homem, R.G. Gomes, M.R. Fagundes-Klen, R. Bergamasco, A.M.S. Vieira, Hybrid treatment of coagulation/flocculation process followed by ultrafiltration in TiO<sub>2</sub>-modified membranes to improve the removal of reactive black 5 dye. *Sci. Total Environ.* **664**, 222–229 (2019)
- P. Jia, Y. Zhou, X. Zhang, Y. Zhang, R. Dai, Cyanobacterium removal and control of algal organic matter (AOM) release by UV/H<sub>2</sub>O<sub>2</sub> pre-oxidation enhanced Fe(II) coagulation. *Water Res.* **131**, 122–130 (2018)
- S. Zhang, S. Zhao, S. Huang, B. Hu, M. Wang, Z. Zhang, L. He, M. Du, Photocatalytic degradation of oxytetracycline under visible light by nanohybrids of CoFe alloy nanoparticles and nitrogen-/sulfur-codoped mesoporous carbon. *Chem. Eng. J.* **420**, 130516 (2021)
- H. Liu, X.-X. Li, X.-Y. Liu, Z.-H. Ma, Z.-Y. Yin, W.-W. Yang, Y.-S. Yu, Schiff-base-rich g-C<sub>3</sub>N<sub>4</sub> supported PdAg nanowires as an efficient Mott–Schottky catalyst boosting photocatalytic dehydrogenation of formic acid. *Rare Met.* **40**, 808–816 (2021)
- L. Bulgariu, D. Bulgariu, Functionalized soy waste biomass—a novel environmental-friendly biosorbent for the removal of heavy metals from aqueous solution. *J. Clean. Prod.* **197**, 875–885 (2018)
- X. Liang, X. Fan, R. Li, S. Li, S. Shen, D. Hu, Efficient removal of Cr(VI) from water by quaternized chitin/branched polyethyleneimine biosorbent with hierarchical pore structure. *Bioresour. Technol.* **250**, 178–184 (2018)
- D. Pradhan, L.B. Sukla, B.B. Mishra, N. Devi, Biosorption for removal of hexavalent chromium using microalgae *Scenedesmus* sp. *J. Clean. Prod.* **209**, 617–629 (2019)
- G. Wang, S. Zhang, P. Yao, Y. Chen, X. Xu, T. Li, G. Gong, Removal of Pb(II) from aqueous solutions by *Phytolacca americana* L. biomass as a low cost biosorbent. *Arab. J. Chem.* **11**, 99–110 (2018)
- M.M. Sobeih, M.F. El-Shahat, A. Osman, M.A. Zaid, M.Y. Nassar, Glauconite clay-functionalized chitosan nanocomposites for efficient adsorptive removal of fluoride ions from polluted aqueous solutions. *RSC Adv.* **10**, 25567–25585 (2020)
- M.Y. Nassar, I.S. Ahmed, H.S. Hendy, A facile one-pot hydrothermal synthesis of hematite (α-Fe<sub>2</sub>O<sub>3</sub>) nanostructures and cephalixin antibiotic sorptive removal from polluted aqueous media. *J. Mol. Liq.* **271**, 844–856 (2018)
- M.Y. Nassar, M. Khatib, Cobalt ferrite nanoparticles via a template-free hydrothermal route as an efficient nano-adsorbent for potential textile dye removal. *RSC Adv.* **6**, 79688–79705 (2016)
- M.Y. Nassar, I.S. Ahmed, M.A. Raya, A facile and tunable approach for synthesis of pure silica nanostructures from rice husk for the removal of ciprofloxacin drug from polluted aqueous solutions. *J. Mol. Liq.* **282**, 251–263 (2019)
- H. Liu, W. Sha, A.T. Cooper, M. Fan, Preparation and characterization of a novel silica aerogel as adsorbent for toxic organic compounds. *Colloids Surf. A* **347**, 38–44 (2009)
- S. Wan, H. Bi, L. Sun, Graphene and carbon-based nanomaterials as highly efficient adsorbents for oils and organic solvents. *J. Nanotechnol. Rev.* **5**, 3–22 (2016)
- R.N. Amador, M. Carboni, D. Meyer, Sorption and photodegradation under visible light irradiation of an organic pollutant by a heterogeneous UiO-67–Ru–Ti MOF obtained by post-synthetic exchange. *J. RSC Adv.* **7**, 195–200 (2017)
- G.-S. Kim, S.-H. Hyun, Synthesis of window glazing coated with silica aerogel films via ambient drying. *J. Non-Cryst. Solids* **320**, 125–132 (2003)
- W. Ackerman, M. Vlachos, S. Rouanet, J. Freundt, Use of surface treated aerogels derived from various silica precursors in translucent insulation panels. *J. Non-Cryst. Solids* **285**, 264–271 (2001)
- T. Asefa, Z. Tao, Biocompatibility of mesoporous silica nanoparticles. *Chem. Res. Toxicol.* **25**, 2265–2284 (2012)
- A.S. Abdel-Bary, D.A. Tolani, M.Y. Nassar, T. Taketsugu, A.M. El-Nahas, Chitosan, magnetite, silicon dioxide, and graphene oxide nanocomposites: synthesis, characterization, efficiency as cisplatin drug delivery, and DFT calculations. *Int. J. Biol. Macromol.* **154**, 621–633 (2020)
- S. Bettini, R. Pagano, G. Bosco, S. Pal, C. Ingrosso, L. Valli, G. Giancane, SiO<sub>2</sub> based nanocomposite for simultaneous magnetic removal and discrimination of small pollutants in water. *Colloids Surf. A* **633**, 127905 (2022)
- P. Feng, H. Chang, X. Liu, S. Ye, X. Shu, Q. Ran, The significance of dispersion of nano-SiO<sub>2</sub> on early age hydration of cement pastes. *Mater. Des.* **186**, 108320 (2020)

40. L. Giraldo, B. López, L. Pérez, S. Urrego, L. Sierra, M. Mesa, Mesoporous silica applications. *Macromol. Symp.* **258**, 129–141 (2007)
41. M.M. Sobeih, M. El-Shahat, A. Osman, M. Zaid, M.Y. Nassar, Glauconite clay-functionalized chitosan nanocomposites for efficient adsorptive removal of fluoride ions from polluted aqueous solutions. *RSC Adv.* **10**, 25567–25585 (2020)
42. J. Aguado, J.M. Arsuaga, A. Arencibia, Adsorption of aqueous mercury(II) on propylthiol-functionalized mesoporous silica obtained by cocondensation. *Ind. Eng. Chem. Res.* **44**, 3665–3671 (2005)
43. J. Gallo, H. Pastore, U. Schuchardt, Silylation of [Nb]-MCM-41 as an efficient tool to improve epoxidation activity and selectivity. *J. Catal.* **243**, 57–63 (2006)
44. R. Jenkins, R.L. Snyder, *Introduction to X-Ray Powder Diffraction* (Wiley, New York, 1996)
45. M.Y. Nassar, M.M. Moustafa, M.M. Taha, Hydrothermal tuning of the morphology and particle size of hydrozincite nanoparticles using different counterions to produce nanosized ZnO as an efficient adsorbent for textile dye removal. *RSC Adv.* **6**, 42180–42195 (2016)
46. M.Y. Nassar, T.Y. Mohamed, I.S. Ahmed, I. Samir, MgO nanostructure via a sol-gel combustion synthesis method using different fuels: an efficient nano-adsorbent for the removal of some anionic textile dyes. *J. Mol. Liq.* **225**, 730–740 (2017)
47. M.P. Gatabi, H.M. Moghaddam, M. Ghorbani, Point of zero charge of maghemite decorated multiwalled carbon nanotubes fabricated by chemical precipitation method. *J. Mol. Liq.* **216**, 117–125 (2016)
48. M.P. Gatabi, H.M. Moghaddam, M. Ghorbani, Efficient removal of cadmium using magnetic multiwalled carbon nanotube nanoadsorbents: equilibrium, kinetic, and thermodynamic study. *J. Nanopart. Res.* **18**, 1–17 (2016)
49. Q. Wang, W. Gao, Y. Liu, J. Yuan, Z. Xu, Q. Zeng, Y. Li, M. Schröder, Simultaneous adsorption of Cu(II) and  $\text{SO}_4^{2-}$  ions by a novel silica gel functionalized with a ditopic zwitterionic Schiff base ligand. *Chem. Eng. J.* **250**, 55–65 (2014)
50. M. Ghaedi, H. Mazaheri, S. Khodadoust, S. Hajati, M. Purkait, Application of central composite design for simultaneous removal of methylene blue and  $\text{Pb}^{2+}$  ions by walnut wood activated carbon. *Spectrochim. Acta A* **135**, 479–490 (2015)
51. Y.-S. Ho, G. McKay, Pseudo-second order model for sorption processes. *Process Biochem.* **34**, 451–465 (1999)
52. Y.-Y. Wang, Y.-X. Liu, H.-H. Lu, R.-Q. Yang, S.-M. Yang, Competitive adsorption of Pb(II), Cu(II), and Zn(II) ions onto hydroxyapatite-biochar nanocomposite in aqueous solutions. *J. Solid State Chem.* **261**, 53–61 (2018)
53. G.D. Halsey, The role of surface heterogeneity in adsorption, in *Advances in Catalysis*, ed. by V.I.K.W.G. Frankenburg, E.K. Rideal (Academic Press, Cambridge, 1952), pp. 259–269
54. S. Liu, Y. Ding, P. Li, K. Diao, X. Tan, F. Lei, Y. Zhan, Q. Li, B. Huang, Z. Huang, Adsorption of the anionic dye Congo red from aqueous solution onto natural zeolites modified with N,N-dimethyl dehydroabietylamine oxide. *Chem. Eng. J.* **248**, 135–144 (2014)
55. X. Zhang, S. Lin, X.-Q. Lu, Z.-L. Chen, Removal of Pb(II) from water using synthesized kaolin supported nanoscale zero-valent iron. *Chem. Eng. J.* **163**, 243–248 (2010)
56. H. Ravishankar, J. Wang, L. Shu, V. Jegatheesan, Removal of Pb(II) ions using polymer based graphene oxide magnetic nanosorbent. *Process Saf. Environ. Prot.* **104**, 472–480 (2016)
57. N.K. Koju, X. Song, Q. Wang, Z. Hu, C. Colombo, Cadmium removal from simulated groundwater using alumina nanoparticles: behaviors and mechanisms. *J. Environ. Pollut.* **240**, 255–266 (2018)
58. G. Bhanjana, N. Dilbaghi, K.-H. Kim, S. Kumar, Carbon nanotubes as sorbent material for removal of cadmium. *J. Mol. Liq.* **242**, 966–970 (2017)

**Publisher's Note** Springer Nature remains neutral with regard to jurisdictional claims in published maps and institutional affiliations.